This article has been accepted for publication in a future issue of this journal, but has not been fully edited. Content may change prior to final publication. Citation information: DOI 10.1109/TPWRD.2019.2952692, IEEE Transactions on Power Delivery

A Unified Control Structure for Grid Connected and Islanded Mode of Operation of Voltage Source Converter based Distributed Generation Units under Unbalanced and Non-linear Conditions

Noel Richard Merritt, Chandan Chakraborty, *Fellow, IEEE*, Prabodh Bajpai, *Senior Member, IEEE*, Bikash. C. Pal, *Fellow, IEEE*

***Abstract*—This manuscript develops a unified control structure for Distributed Generation (DG) units based on Voltage Source Converters considering unbalanced and non-linear operating conditions. This control structure works for both the Islanded and the Grid-connected modes of operation of the Micro-Grid (MG). The objective of this control scheme is to regulate the line currents of the DG unit in such a manner that the voltage at the Point of Common Coupling (PCC) remains balanced despite the line currents of the DG unit being unbalanced and distorted. Multiple adaptive P-R controllers have been proposed for the current control loop of the Voltage Source Converter (VSC). These controllers have been implemented with resettable integrators so as to limit the DC components in the post fault current of the VSC. The Battery Energy Storage System (BESS) is interfaced to the DC link of the VSC through bi-directional dc-dc converters. An improved control structure for the bi-directional dc-dc converter has been developed. The effectiveness of these control structures have been presented and tested in PSCAD/EMTDC in an IEEE 34 node distribution system model being fed by two identical DG units.**

***Index Terms*—Voltage Source Converter (VSC), Bi-directional dc-dc converter, Micro-Grid (MG), Generalized Integrator (GI).**

I. Introduction

THE concept of the Micro-Grid (MG) involves the use of Distributed Generation (DG) units delivering power to low voltage distribution systems so as to ensure a balance between the generation and load within the local network [1]. The DG units within the MG usually operate differently when the MG is in the Islanded Mode (ISM) and in the Grid-Connected Mode (GCM) of operation, and so the researchers felt the need for utilizing two distinct sets of control structures for the DG unit [2] – [4]. However it is clear that the use of two distinct sets of controllers makes things complicated and so, references [5], [6] presented a unified control structure that works for both the ISM and the GCM of operation. Although reference [5] presented a common control scheme that works for both the GCM and ISM of operation, the results for the GCM and ISM of operation have been presented separately, a transition from the GCM to ISM of operation and vice-versa hasn't been demonstrated. Also, unbalanced and linear loads were considered with the traditional dq-frame control. Reference [6] dealt with unbalanced conditions very effectively, but the method for separating the sequence components under non-linear conditions would involve a laborious procedure. References [7] – [9] have presented control structures considering non-linear loads and the Total Harmonic Distortion (THD) of the PCC voltage with these schemes has been reduced to a great extent. However references [7] – [9] have considered very small systems with the load (non-linear and balanced at harmonic frequencies) very close to the DG units and also haven't tested their algorithms for fault conditions. References [7] and [9] have considered only the ISM of operation, while in reference [8] two entirely different sets of control structures have been utilized for the ISM and the GCM of operation (2nd order Sliding Mode Control (SMC) for VSC current control in the GCM and 3rd order SMC for PCC voltage control in the ISM). Although SMC is very effective, the serious disadvantage involved is the chattering effect.

In order to smoothen the power fluctuations from the PV arrays, a Battery Energy Storage System (BESS) has been utilized and it is usually interfaced to the DC link of the VSC through a bi-directional dc-dc converter (unlike in reference [6], where the BESS has been interfaced directly to the DC link of the VSC, which may not be practically feasible). As far as controlling the bi-directional dc-dc converter is concerned, references [10] and [11] have presented a closed loop current control structure for a full bridge converter, while the outer loop voltage control to decide the reference command of the current control structure has not been presented and therefore only the constant current control mode of operation is possible. Reference [12] has presented the inner loop current control and the outer loop voltage control based on the small signal model. The drawback of this control structure is that both the inner loop current control and the outer loop voltage control models do not have an open loop pole at the origin and therefore in practice there will exist a certain amount of steady state error. References [13] – [16] have presented a similar control structure (inner loop current control and the outer loop voltage

Manuscript received June 10, 2019; revised September 15, 2019; accepted November 2, 2019.

Noel Richard Merritt, Dr. Chandan Chakraborty and Dr. Prabodh Bajpai are with the Department of Electrical Engineering, Indian Institute of Technology Kharagpur, Kharagpur 721302, India (e-mail: noelrichard.merritt@gmail.com; chakraborty@ieee.org; pbajpai@ee.iitkgp.ernet.in).

Dr. Bikash. C. Pal is with the Department of Electrical and Electronic Engineering, Imperial College London, London SW72BT, U.K (email: b.pal@imperial.ac.uk).

Color versions of one or more of the figures in this paper are available online at http://ieeexplore.ieee.org.

Digital Object Identifier

This article has been accepted for publication in a future issue of this journal, but has not been fully edited. Content may change prior to final publication. Citation information: DOI 10.1109/TPWRD.2019.2952692, IEEE Transactions on Power Delivery

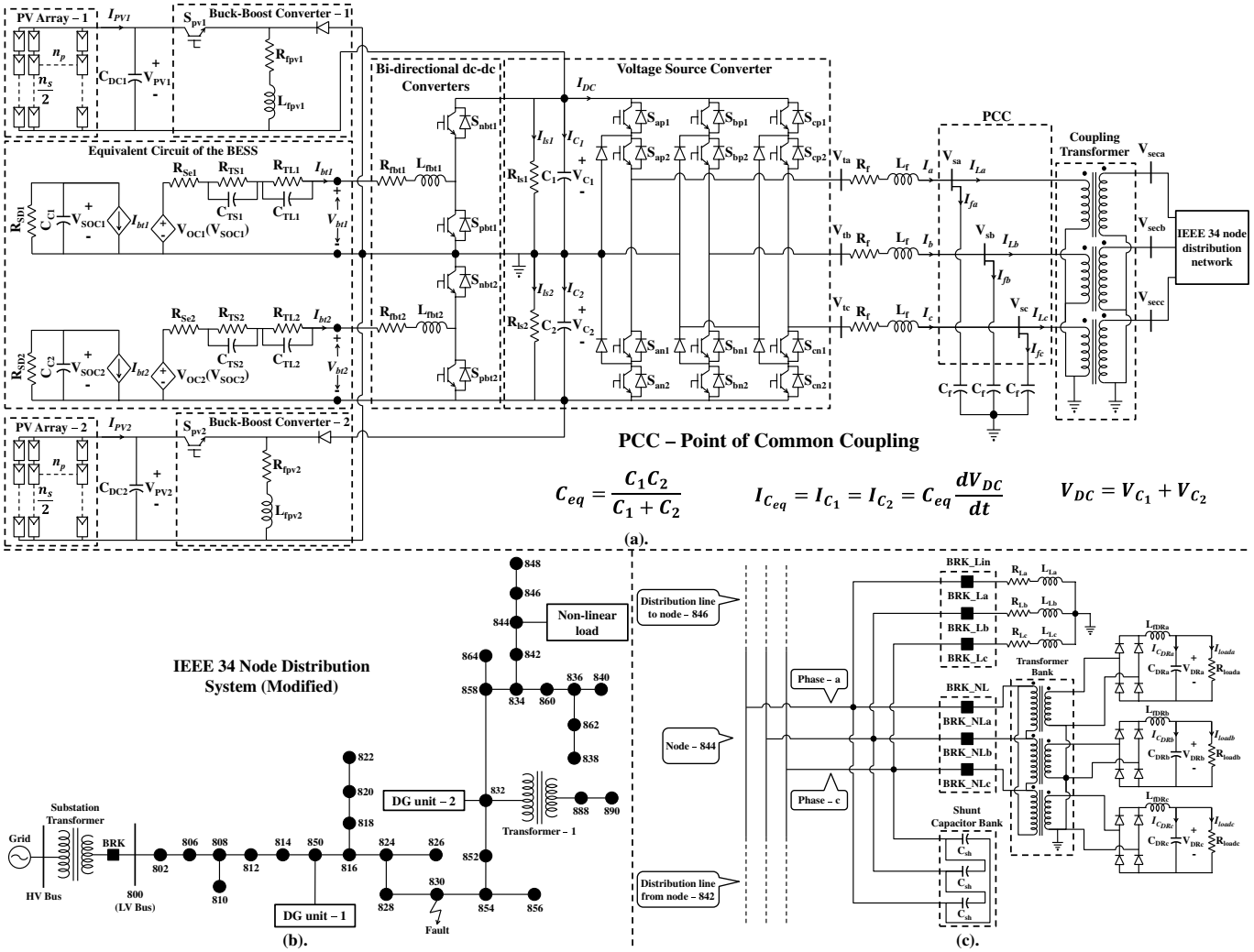

$$C_{eq} = \frac{C_1 C_2}{C_1 + C_2} \qquad I_{C_{eq}} = I_{C_1} = I_{C_2} = C_{eq}\frac{dV_{DC}}{dt} \qquad V_{DC} = V_{C_1} + V_{C_2}$$

Fig. 1: (a). Circuit diagram of the DG unit with BESS and PV Arrays; (b). IEEE 34 node Distribution System (Modified) [17]; (c). Loads connected at node-844 of the IEEE 34 node Distribution System.

control) without feed-forward compensation. The main issue is that the absence of feed-forward compensation will make the overall closed loop control system sensitive to disturbance inputs present in the open loop control models.

Hence the aim of the research presented in this manuscript is to study the impact of non-linear loads on the dynamics of a large MG being fed by multiple DG units; to present a unified control scheme for the VSC that works for both the ISM and the GCM of operation of the MG; and to present an improved control scheme (employing feed-forward compensation) for the bi-directional dc-dc converter (interfacing the BESS with the DC link of the VSC), so as to achieve the following targets:

- To maintain balanced and sinusoidal voltages at the PCC of the DGs, considering unbalanced and non-linear loads (with unbalance even at harmonic frequencies).
- To limit unsymmetrical fault currents so as to protect the power electronic switches.
- To utilize the same control structure for both ISM and GCM of operation of the MG.
- To control the bi-directional dc-dc converter in such a manner that the BESS will be able to handle the power fluctuations from the PV arrays and to maintain the DC link capacitor voltages constant at all times.

Multiple adaptive P-R controllers have been chosen for the inner loop VSC current control. These controllers have been introduced based on the concept of the GI [24] and have been implemented with resettable integrators so as to limit the DC components in the post fault current of the VSC. The outer loop PCC voltage control (dq-frame and zero sequence) will decide the references of the inner loop current control. The real power and frequency control schemes in cascade [5], [6] (these references have primarily focused on linear loads and the same concept is extended to non-linear loads in this manuscript) will decide the reference for the q-axis component of the PCC voltage control.

II. System Description

The circuit diagram of the DG unit is shown in Fig. 1a. The VSC (represented by a three level Neutral Point Clamped (NPC) converter along with the LC filter) is interfaced to the MG through a coupling transformer. Two identical bi-directional dc-dc converters interface two identical BESS

This article has been accepted for publication in a future issue of this journal, but has not been fully edited. Content may change prior to final publication. Citation information: DOI 10.1109/TPWRD.2019.2952692, IEEE Transactions on Power Delivery

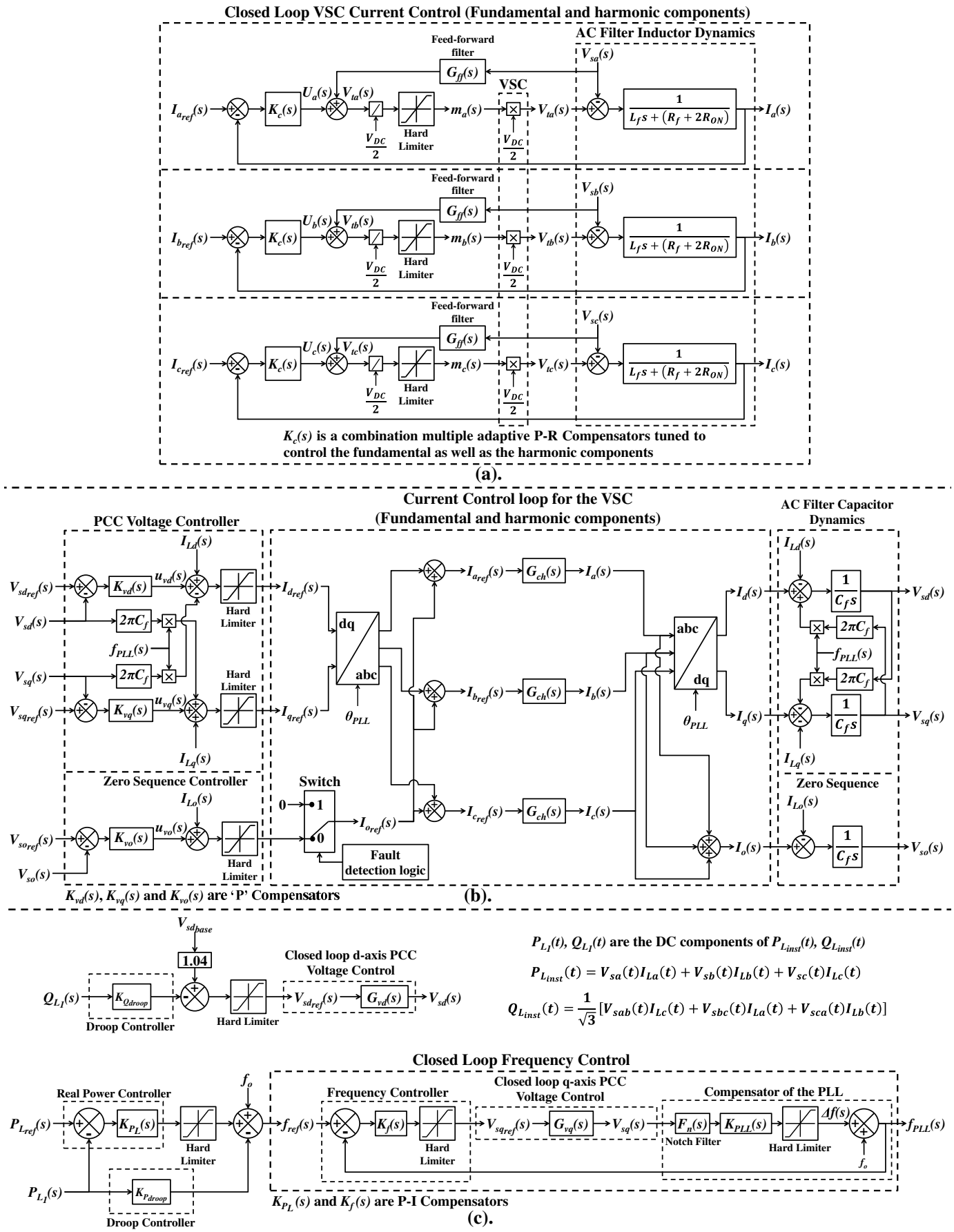

Fig. 2: (a). VSC Current Control Structure for the VSC of the DG unit; (b). PCC Voltage Control Structure for the VSC of the DG unit (c). Outer Loop Control Schemes to decide the references of the PCC Voltage Control loop in dq-frame.

This article has been accepted for publication in a future issue of this journal, but has not been fully edited. Content may change prior to final publication. Citation information: DOI 10.1109/TPWRD.2019.2952692, IEEE Transactions on Power Delivery

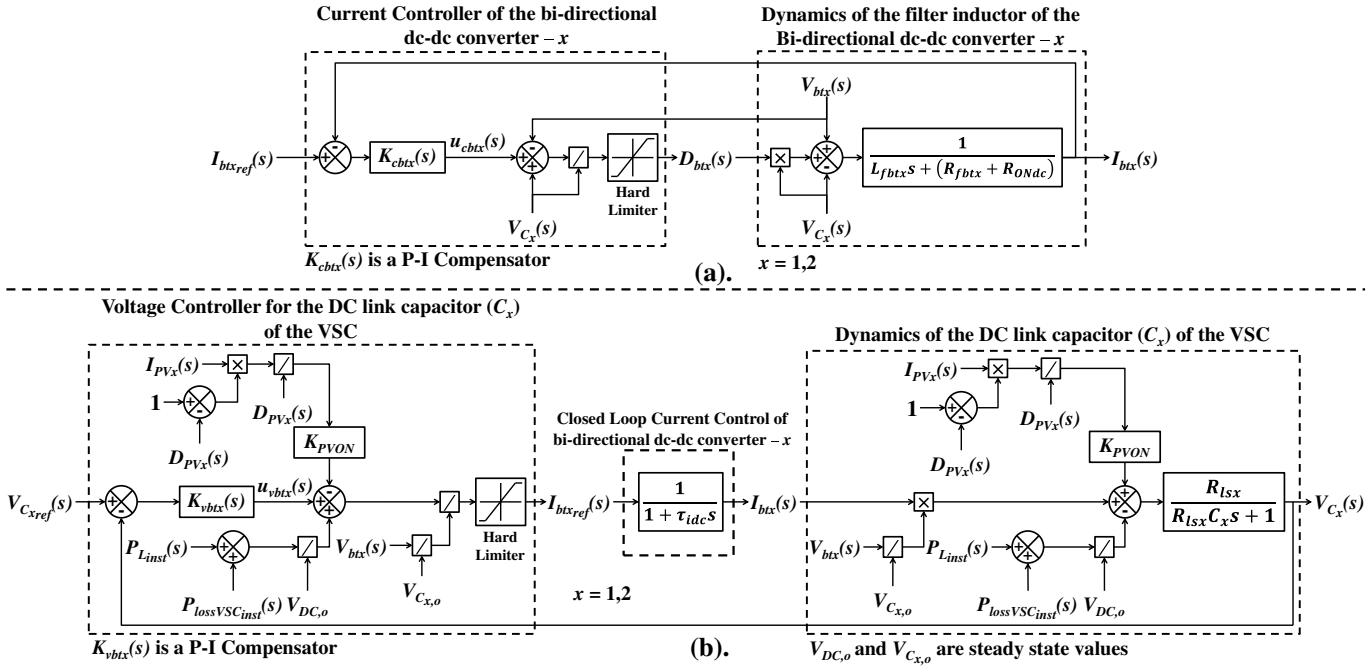

Fig. 3: (a). Closed loop current control for the bi-directional dc-dc converter; (b). Closed loop voltage control for the bi-directional dc-dc converter.

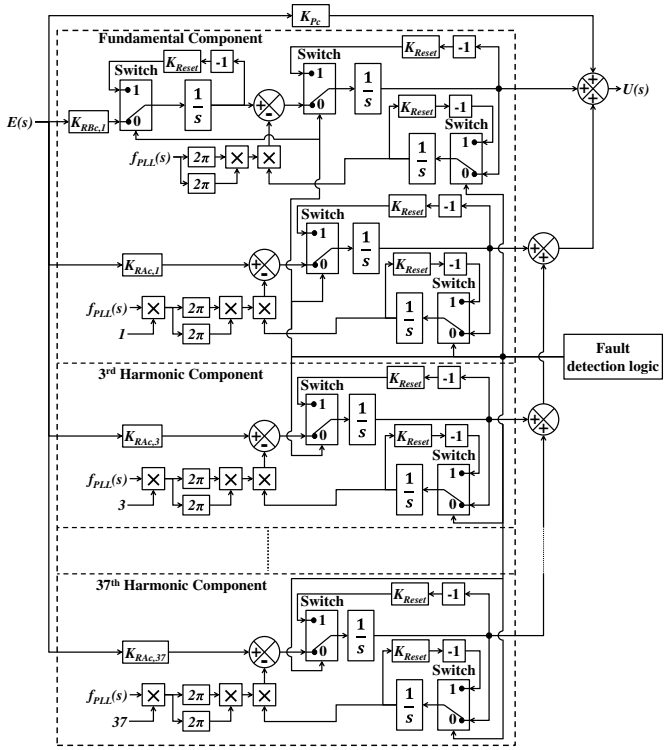

Fig. 4: Adaptive P-R Control implemented with resettable integrators.

banks (which are represented by the Thevenin's equivalent circuit [18]) with the DC link capacitors (C_1 and C_2) of the VSC. Two identical Buck-Boost converters interface two identical PV arrays with the DC link capacitors (C_1 and C_2) of the VSC. The duty ratio of the Buck-Boost converters ($D_{PV1}(t)$ and $D_{PV2}(t)$) is regulated accordingly so that the PV system will operate at the Maximum Power Point (MPP). The VSC is regulated accordingly so that it delivers power to the MG as per the load demand (if the MG is operating in the ISM) or according to the reference command (if the MG is operating in the GCM). The duty ratio of the bi-directional dc-dc converters is regulated accordingly so that the BESS banks will be able to handle the mismatch between the power delivered by the VSC to the MG and the power generated by the PV arrays. Two identical DG units are interfaced to the modified version of the IEEE 34 node distribution system (the circuit diagram has been displayed in Fig. 1b) at nodes '832' and '850'. Fig. 1c shows the connection of the spot linear load and the non-linear load at node-844.

III. Control Structures

A. Control Structure for the VSC:

The aim of the VSC current control loop (displayed in Fig. 2a) is to control the VSC currents (fundamental and harmonic components) in abc-frame to the respective reference commands by varying the modulation index of the individual phases. Feed-forward compensation has been introduced based on the open loop control model (which is obtained by applying Kirchhoff's Voltage Law (KVL) across the AC filter reactor). Multiple adaptive P-R controllers (shown in Fig. 4) for controlling the fundamental and the harmonic components separately and independently are employed. Therefore the compensator '$K_c(s)$' in Fig. 2a can be mathematically represented as follows:

$$K_c(s) = K_{Pc} + \sum_{i=1}^{n}\left[K_{RAc,(2i-1)}\left(\frac{s}{s^2+\left((2i-1)\,\omega_{PLL}\right)^2}\right)\right] + K_{RBc,1}\left(\frac{1}{s^2+\omega_{PLL}^2}\right) \quad (1)$$

This article has been accepted for publication in a future issue of this journal, but has not been fully edited. Content may change prior to final publication. Citation information: DOI 10.1109/TPWRD.2019.2952692, IEEE Transactions on Power Delivery

Where, 'ω_{PLL}' is the tracked angular frequency of the PLL (not shown in this manuscript due to brevity) and 'n' is chosen as '19', so that harmonics up to the 37th harmonic can be regulated. The parameters of '$K_c(s)$' have been chosen as follows:

$$K_{Pc} = \frac{2L_f}{\tau_{c,1}}; K_{RBc,1} = \frac{(R_f + 2R_{ON})}{\tau_{c,1}^2} - \omega_{PLL}^2 K_{Pc} \quad (2)$$

$$K_{RAc,(2i-1)} = \frac{L_f}{\tau_{c,(2i-1)}^2} + \frac{2\left(R_f + 2R_{ON}\right)}{\tau_{c,(2i-1)}} \quad (3)$$

Where, '$\tau_{c,(2i-1)}$' is the desired time constant for the $(2i-1)^{\text{th}}$ harmonic component. The expressions for 'K_{Pc}' and '$K_{RBc,1}$' in the equations above are specifically meant for the fundamental component, while the expression for '$K_{RAc,(2i-1)}$' is meant for the fundamental as well as the harmonic components. The resultant closed loop transfer function while considering harmonics up to the 13th harmonic is as follows:

$$\frac{I_a(s)}{I_{a_{ref}}(s)} = \frac{I_b(s)}{I_{b_{ref}}(s)} = \frac{I_c(s)}{I_{c_{ref}}(s)} = G_{ch}(s) = \frac{Num_c(s)}{Den_c(s)} \quad (4)$$

Where $Num_c(s)$ and $Den_c(s)$ have been displayed in equations (A1) and (A2) in the Appendix respectively.

B. Deciding the references for the VSC Current Control:

Based on Fig. 2b, the PCC voltage control in dq-frame along with the zero sequence voltage control will decide the reference commands of the VSC current control loop. The Reactive Power–Voltage Droop control structure decides the reference command for the d-axis component of the PCC Voltage ($V_{sd_{ref}}(s)$). The Real Power control structure along with the frequency control structure in cascade decide the reference command for the q-axis component of the PCC Voltage ($V_{sq_{ref}}(s)$). The implementation of this cascaded control scheme makes the overall control structure of the VSC independent of the knowledge of the mode of operation of the MG. In the GCM of operation of the MG, the real power compensator '$K_{P_L}(s)$' will regulate the reference command of the frequency control loop '$f_{ref}(s)$' in such a manner that the real power supplied by the VSC of the DG unit '$P_{L_1}(s)$' will match the desired reference command '$P_{L_{ref}}(s)$'. In the ISM of operation of the MG, the real power compensator '$K_{P_L}(s)$' will get saturated either at -0.1 or at 0.2 (because the frequency limits chosen are between 59.8 Hz to 60.2 Hz) depending on the error fed to the compensator and the droop control scheme '$K_{P_{droop}}P_{L_1}(s)$' (shown in Fig. 2c) will now take charge in deciding the reference command for the frequency control loop '$f_{ref}(s)$'.

Based on the open loop PCC voltage control model in Fig. 2b, it is clear that there is a pole at the origin. Also, all the harmonic components will appear in the feed-forward terms $I_{Ld}(s), I_{Lq}(s)$ and $I_{Lo}(s)$. Therefore it is sufficient for $K_{vd}(s)$, $K_{vq}(s)$ and $K_{vo}(s)$ to be purely proportional compensators (each of gain 'K_v'). Therefore the resultant closed loop transfer function will be:

$$\frac{V_{sd}(s)}{V_{sd_{ref}}(s)} = \frac{V_{sq}(s)}{V_{sq_{ref}}(s)} = \frac{V_{so}(s)}{V_{so_{ref}}(s)} = \frac{G_{ch}(s)K_v}{C_f s + G_{ch}(s)K_v} \quad (5)$$

C. Control of bi-directional dc-dc converters:

The aim of this control scheme is to control the bi-directional dc-dc converters of Fig. 1a, so that the BESS will be able to handle the mismatch between the power delivered by the VSC to the MG and the power generated by the PV arrays (the control structure has not been shown in this manuscript due to brevity). Therefore the PV arrays will always operate at MPP as long as the BESS is not fully charged.

1) Inner loop current control: The aim of the closed loop current control (Fig. 3a) is to control the filter reactor current of each of the bi-directional dc-dc converters to the respective reference commands, by varying the duty ratio of the converter ($D_{btx}(t)$, where $x = 1, 2$). Feed-forward compensation has been introduced based on the model for the open loop control (which can be obtained by applying KVL across the filter reactor 'L_{fbtx}' and the IGBT switches in the ON state). P-I compensators have been chosen for each of the control loops. The zero of the P-I compensator (equation (7)) has been chosen so that it coincides with the pole of the open loop control model. Therefore the resultant closed loop system is a 1st order system with the pole far away from the origin (towards the left side along the real axis) resulting in a fast and stable response. The compensators of the current control loops are (where $x = 1, 2$):

$$K_{cbtx}(s) = K_{P_{cx}}\left(\frac{s + z_{cx}}{s}\right) = K_{P_{cx}} + \frac{K_{I_{cx}}}{s} \quad (6)$$

Where 'z_{cx}' has been chosen as follows:

$$z_{cx} = \left(\frac{K_{I_{cx}}}{K_{P_{cx}}}\right) = \left(\frac{R_{fbtx} + R_{ON_{DC}}}{L_{fbtx}}\right) \quad (7)$$

2) Outer loop voltage control: By applying Kirchoff's Current Law (KCL) at the DC link Capacitors of the VSC (for the circuit shown in Fig. 1a), the model for the open loop control can be obtained and the equation for Converter-*x* will be (where $x = 1, 2$):

$$I_{C_x}(t) = C_x\frac{dV_{C_x}(t)}{dt} = \underbrace{\left(\frac{V_{btx}(t)}{V_{C_x}(t)}\right)I_{btx}(t)}_{\text{Bi-directional dc-dc Converter-}x} + \underbrace{K_{PV_{ON}}I_{PVx}(t)\left(\frac{1 - D_{PVx}(t)}{D_{PVx}(t)}\right)}_{\text{PV Array-}x} - \underbrace{\left(\frac{P_{L_{inst}}(t) + P_{lossVSC_{inst}}(t)}{V_{DC}(t)}\right)}_{\text{Resultant DC link current}} - \frac{V_{C_x}(t)}{R_{lsx}} \quad (8)$$

Where,

This article has been accepted for publication in a future issue of this journal, but has not been fully edited. Content may change prior to final publication. Citation information: DOI 10.1109/TPWRD.2019.2952692, IEEE Transactions on Power Delivery

$$K_{PV_{ON}} = \begin{cases} 1 & \text{if the PV system is ON} \\ 0 & \text{if the PV system is OFF} \end{cases} \quad (9)$$

The aim of the closed loop voltage control (Fig. 3b) is to control the voltage of the DC link capacitor of the VSC (C_x) to the reference command of the inner loop current control ($I_{btx_{ref}}(t)$). Feed-forward compensation has been introduced based on the open loop control model (equation (8)). P-I compensators have been chosen for each of the control loops. The zero of the P-I compensator (equation (11)) has been chosen so that it either coincides or is placed very close to the pole of the open loop control model. Therefore the resultant closed loop system is a 2nd order system (stable for all values of '$K_{P_{vx}}$'). The compensators of the voltage control loops are:

$$K_{vbtx}(s) = K_{P_{vx}}\left(\frac{s+z_{vx}}{s}\right) = K_{P_{vx}} + \frac{K_{I_{vx}}}{s} \quad (10)$$

Where 'z_{vx}' has been chosen as follows:

$$z_{vx} = \left(\frac{K_{I_{vx}}}{K_{P_{vx}}}\right) = \left(\frac{1}{R_{lsx}C_x}\right) \quad (11)$$

The Closed loop transfer function for the voltage control loops of Converter-*x* is as follows (for perfect Pole-Zero cancellation):

$$\frac{V_{C_x}(s)}{V_{C_{x_{ref}}}(s)} = \frac{\left(\frac{K_{P_{vx}}K_{P_{cx}}}{C_x L_{fbtx}}\right)}{s^2 + \left(\frac{K_{P_{cx}}}{L_{fbtx}}\right)s + \left(\frac{K_{P_{vx}}K_{P_{cx}}}{C_x L_{fbtx}}\right)} \quad (12)$$

The Closed loop transfer function for the voltage control loops of Converter-*x* is as follows (for imperfect Pole-Zero cancellation):

$$\frac{V_{C_x}(s)}{V_{C_{x_{ref}}}(s)} = \frac{N_{vx}(s)}{D_{vx}(s)} \quad (13)$$

Where,

$$N_{vx}(s) = K_{P_{vx}}R_{lsx}\left(s + \frac{K_{I_{vx}}}{K_{P_{vx}}}\right) \quad (14)$$

$$D_{vx}(s) = R_{lsx}C_x\left(\frac{L_{fbtx}}{K_{P_{cx}}}\right)s^3 + \left[\left(\frac{L_{fbtx}}{K_{P_{cx}}}\right) + R_{lsx}C_x\right]s^2 + \left(1 + K_{P_{vx}}R_{lsx}\right)s + K_{I_{vx}}R_{lsx} \quad (15)$$

IV. Simulation Results

Two identical DG units have been interfaced to the modified version of the IEEE 34 node distribution system at nodes '832' and '850'; and implemented in PSCAD/EMTDC environment. The parameters of the compensators along with the parameters of a single DG unit are displayed in Table A2 and Table A3 in the Appendix respectively. The PV system is rated at 2.3 MW at STC (for each of the DG units). For the Real Power Control structure of each of the DG units, the reference command has been set at 1.15 MW.

TABLE I: Steady state values of % THD at t=3.0s for the results of Section IV-A

Location	Variables	% THD
DG unit-1	V_{sa}, V_{sb}, V_{sc}	0.1556 %, 0.1205 %, 0.1323 %
	I_{La}, I_{Lb}, I_{Lc}	9.1071 %, 12.7654 %, 10.4523 %
DG unit-2	V_{sa}, V_{sb}, V_{sc}	0.1835 %, 0.1140 %, 0.1389 %
	I_{La}, I_{Lb}, I_{Lc}	11.7821%, 15.6687 %, 12.5278 %
Node-800	$V_{800a}, V_{800b}, V_{800c}$	2.6599 %, 3.4994 %, 2.2715 %
Node-830	$V_{830a}, V_{830b}, V_{830c}$	2.8504 %, 3.8199 %, 2.4979 %
Node-832	$V_{832a}, V_{832b}, V_{832c}$	3.1698 %, 4.3056 %, 2.8336 %
Node-844	$V_{844a}, V_{844b}, V_{844c}$	3.4540 %, 4.7209 %, 3.1201 %
Node-848	$V_{848a}, V_{848b}, V_{848c}$	3.5022 %, 4.7878 %, 3.1663 %
Node-850	$V_{850a}, V_{850b}, V_{850c}$	2.5691 %, 3.3799 %, 2.2117 %
Node-862	$V_{862a}, V_{862b}, V_{862c}$	3.4190 %, 4.6669 %, 3.0816 %

A. ISM of operation of the MG–Response to a Load Transient (Unbalanced linear load to unbalanced non-linear load):

The MG has been initially working in the ISM (after performing a black start under default loading conditions as reported in [17]). At t=1.0s, the spot load (linear) at node-844 has been switched OFF by opening the circuit breaker 'BRK_Lin' (shown in Fig. 1c), and a three phase non-linear load (shown in Fig. 1c with the parameters mentioned in Table A1 in the Appendix) connected at the same node, has been switched ON (The power consumed by this load has been shown in Fig. 5h) by closing the circuit breaker 'BRK_NL'. From Fig. 5a, it is clear that the voltages at the PCC of DG unit-2 are balanced and sinusoidal even though the currents supplied by DG unit-2 (shown in Fig. 5b) are unbalanced and non-linear (The THD of the PCC voltages and line currents of both the DG units are shown in Table I). Therefore, it can be concluded that the PCC voltage control structures (the dq-frame and the zero sequence control) are able to regulate the PCC voltages to the reference commands (as shown in Fig. 5j, 5k, 5l). Based on Fig. 5c it is clear that the frequency control structure is able to regulate the frequency of DG unit-2 to the reference command. The instantaneous values of real and reactive power delivered by DG unit-2 are displayed in Fig. 5d. Based on Fig. 5e it can be observed that the BESS is capable of handling the imbalance between the power delivered (to the MG) by the VSC and the power generated by the PV system. This has been made possible because, the control structure for the bi-directional dc-dc converter has been able to control the BESS currents (Fig. 5i) and the DC link capacitor voltages (Fig. 5f) to the respective reference commands. Therefore the PV arrays will always operate at MPP until the BESS gets fully charged. Table I shows the THD of the Phase voltages at various points in the network. The THD is different in the three phases which clearly indicates that there is unbalance even at harmonic frequencies. It also can be observed that the THD of the voltages at the far ends of the feeder is much higher when compared to the nodes that are closer to the DG units (Fig. 5g shows the Phase voltages at node-844). The reason for this condition is that even though the PCC voltages of the DG units are balanced and sinusoidal, the voltages at the far ends

This article has been accepted for publication in a future issue of this journal, but has not been fully edited. Content may change prior to final publication. Citation information: DOI 10.1109/TPWRD.2019.2952692, IEEE Transactions on Power Delivery

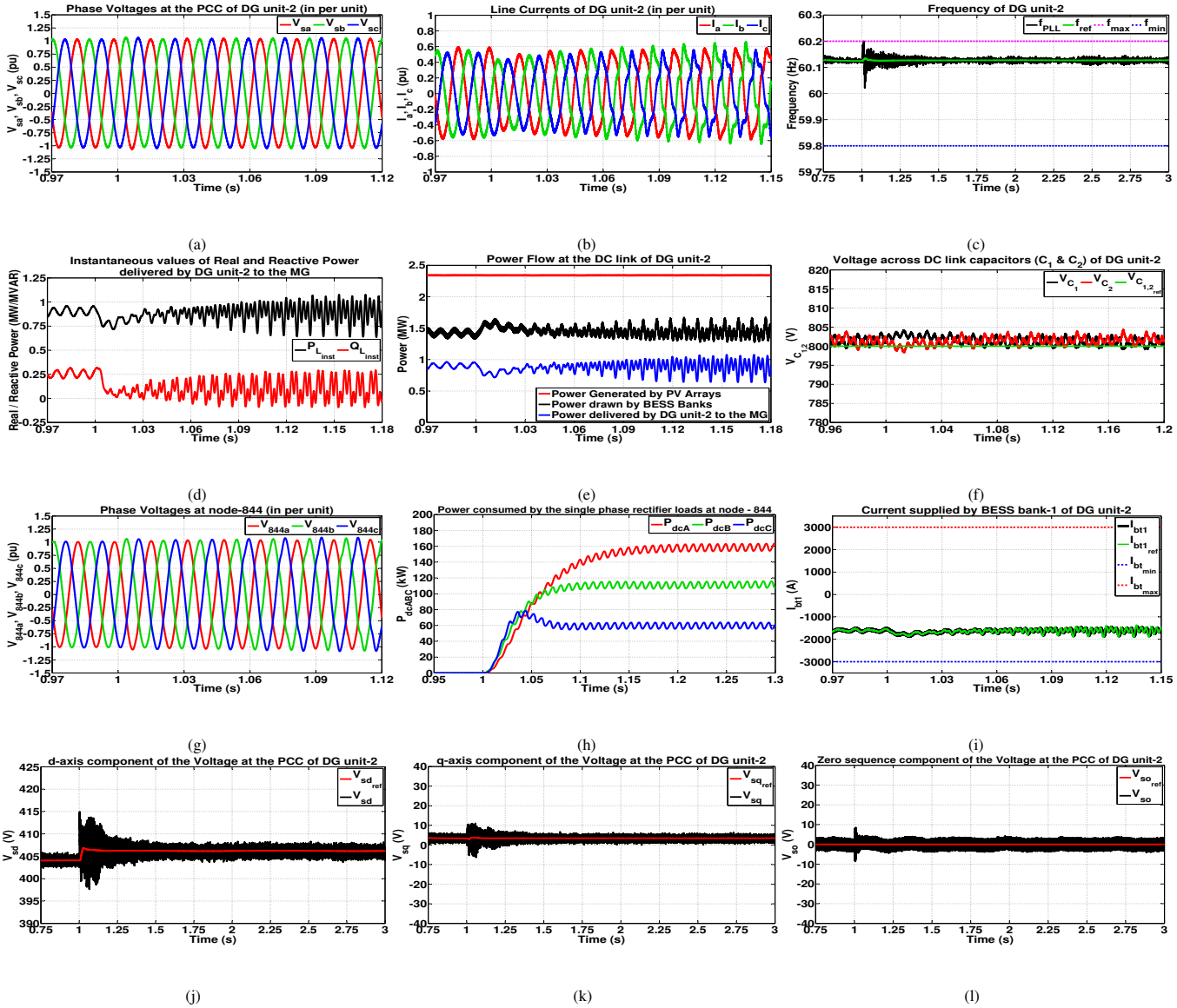

Fig. 5: ISM of operation of the MG–Response to a Load Transient (Unbalanced linear load to unbalanced non-linear load).

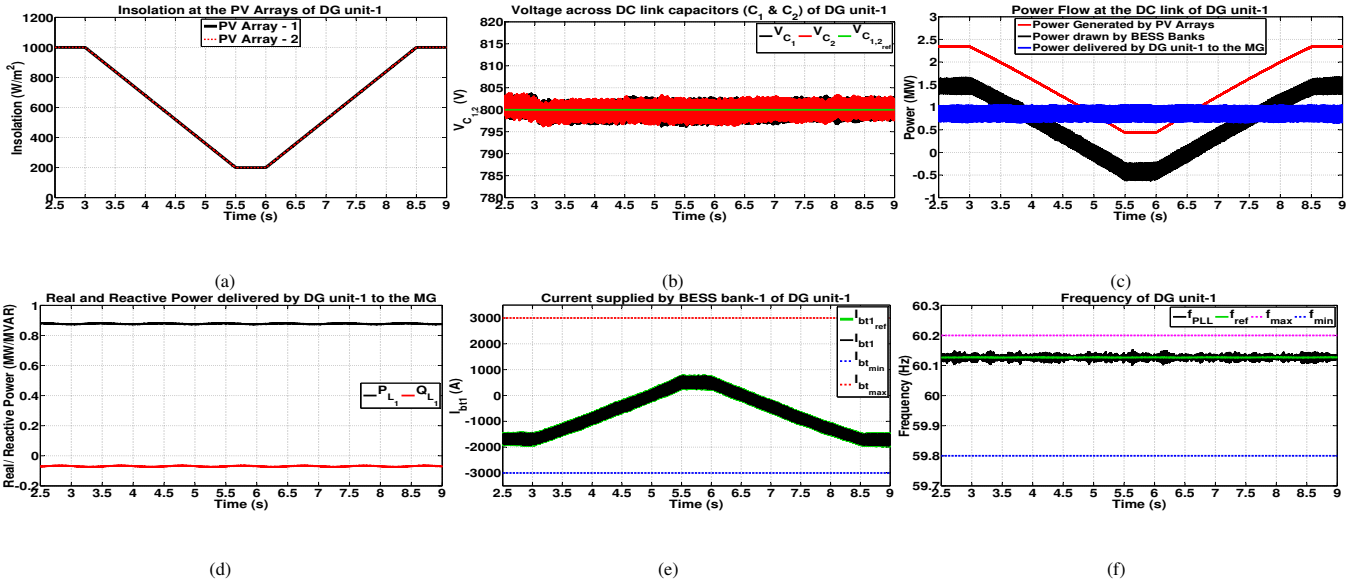

Fig. 6: ISM of operation of the MG–Response to variation in insolation.

This article has been accepted for publication in a future issue of this journal, but has not been fully edited. Content may change prior to final publication. Citation information: DOI 10.1109/TPWRD.2019.2952692, IEEE Transactions on Power Delivery

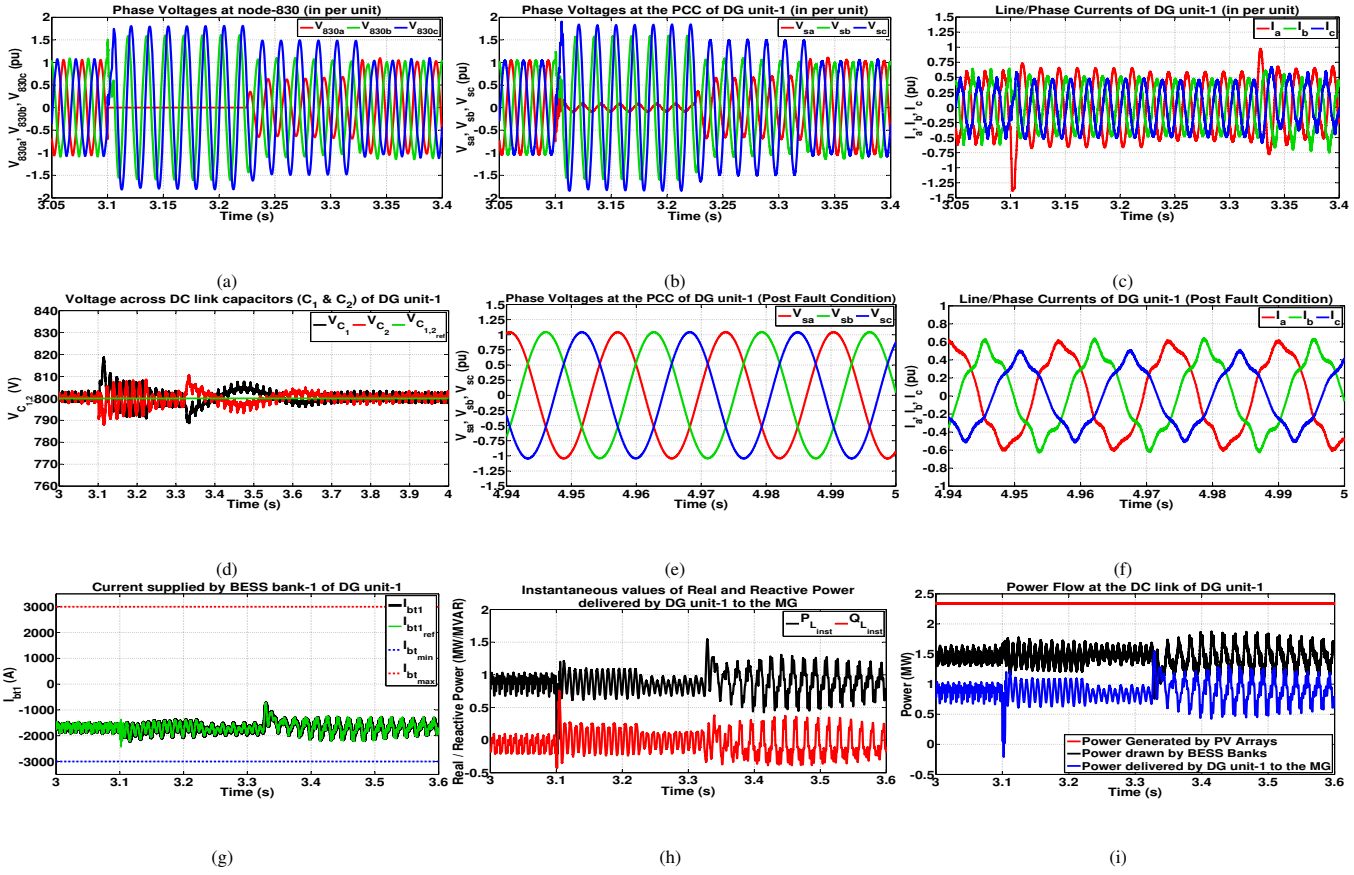

Fig. 7: ISM of operation of the MG–Response to a temporary network transient (Single Line to Ground Fault).

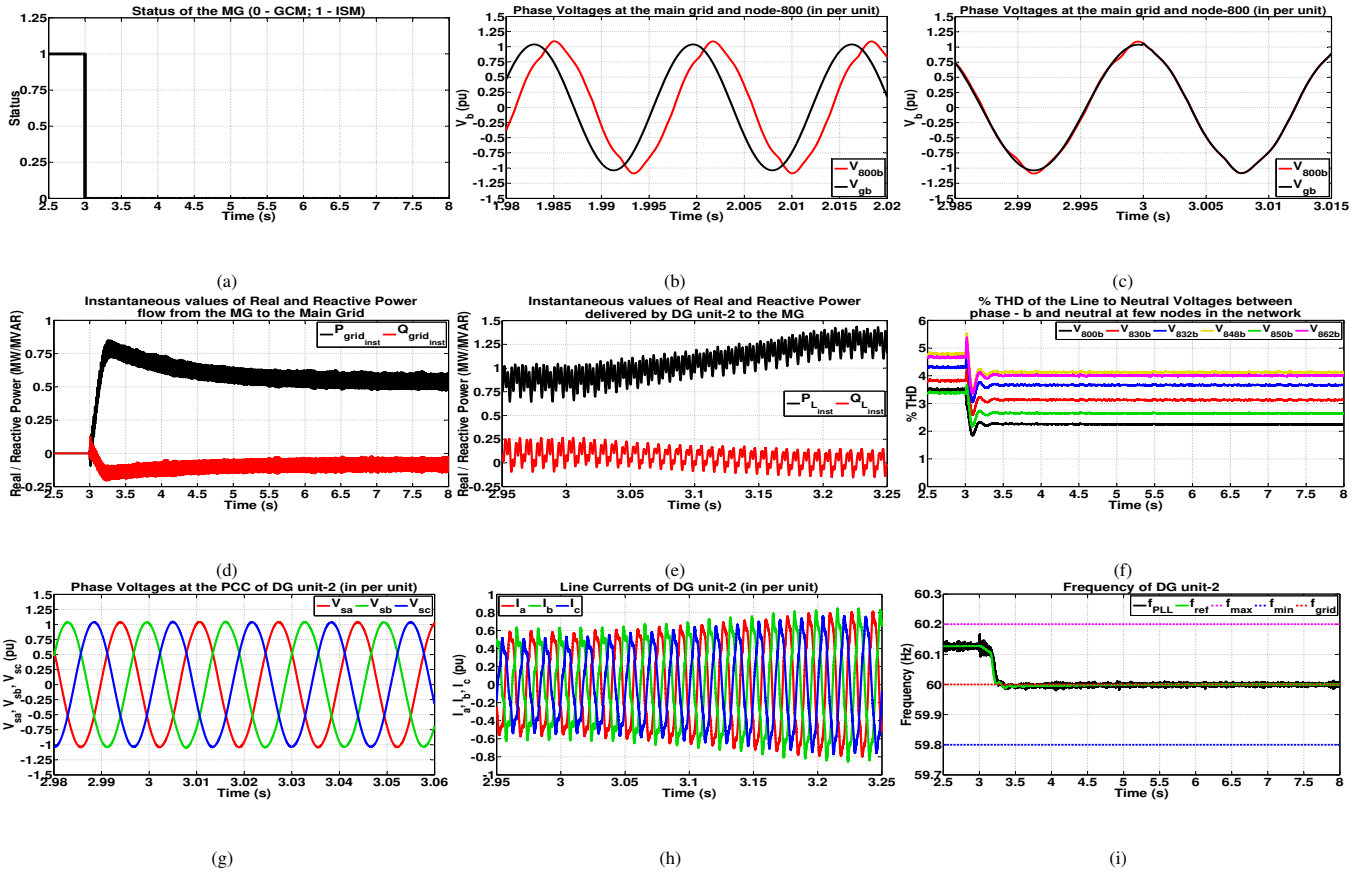

Fig. 8: Synchronization of the MG to the main grid.

This article has been accepted for publication in a future issue of this journal, but has not been fully edited. Content may change prior to final publication. Citation information: DOI 10.1109/TPWRD.2019.2952692, IEEE Transactions on Power Delivery

of the feeder get distorted because, the voltage drops across the feeder are non-sinusoidal because of the non-sinusoidal currents flowing in the feeder.

B. ISM of operation of the MG–Response to variation in insolation:

The MG has been working in the ISM after the change in load from linear to non-linear (in Section IV-A). At t=3.0s, the insolation level for the PV arrays of both the DG units has been ramped down from 1000 W/m^2 to 200 W/m^2 and then again ramped up to 1000 W/m^2 (as shown in Fig. 6a for the PV arrays of DG unit-1). Based on Fig. 6c it can be observed that the BESS is capable of handling the imbalance between the power delivered (to the MG) by the VSC and the power generated by the PV arrays. Therefore the PV system operates at MPP even under varying insolation and the VSC supplies constant power to the MG (as shown in Fig. 6d because there is no change (in load) or a disturbance in the MG). From Fig. 6b, it is clear that the outer loop voltage control structure for the bi-directional dc-dc converter is capable of controlling the DC link capacitor voltage to the reference command. As a result, the reference for the inner loop current control structure to control the BESS currents has been suitably varied (shown in Fig. 6e) by means of feed-forward compensation so as to achieve this target. Fig. 6f shows the frequency of DG unit-1.

C. ISM of operation of the MG–Response to a temporary network transient (Single Line to Ground Fault):

The MG has been working in the ISM after the change in load from linear to non-linear (in Section IV-A). At t=3.1s, the MG has been subjected to a single line to ground fault for a period of 0.12s, at node-830 (displayed in Fig. 7a). The simulation results for this case have been displayed in Fig. 7. The PCC voltage and the phase currents of DG unit-1 have been displayed in Fig. 7b and Fig. 7c respectively. The steady state values of the PCC voltage of DG unit-1 and the phase currents of DG unit-1 have been displayed in Fig. 7e and Fig. 7f respectively. From Fig. 7c, it can be clearly observed that there is an initial overshoot in the line current because the resonant part of the P-R controller is still active. It takes around 0.5 to 1 cycles for the fault detection logic (not presented in this manuscript due to brevity) to detect the fault. Once the fault is detected, the resonant part of the P-R controller will be disabled (for the purpose of reducing the DC components in the post fault current). Thus, the initial overshoot cannot be avoided. Fig. 7h shows the instantaneous values of real and reactive power delivered by DG unit-1. Based on Fig. 7i it can be observed that the BESS is capable of handling the imbalance between the power delivered (to the MG) by the VSC and the power generated by the PV system even during fault condition. The control structure for the bi-directional dc-dc converter has been able to control the BESS currents (Fig. 7g) and the DC link capacitor voltages (Fig. 7d) to the respective reference commands. Therefore even during fault condition, the PV arrays will always operate at MPP.

D. Synchronization of the MG to the main grid:

The MG has been working in the ISM after the change in load from linear to non-linear (in Section IV-A). Between t=1.98s and t=2.02s, a considerable phase difference between the grid voltage and the voltage at node-800 can be observed (Fig. 8b) and so the MG cannot be synchronized to the main grid at this point of time. At t=3.0s, a negligible phase difference between the main grid and the MG can be observed (Fig. 8c). Therefore, at this point of time, the circuit breaker 'BRK' has been closed (which means that the MG and the main grid are synchronized) which can be obviously inferred from Fig. 8a, Fig. 8c, and Fig. 8d. The grid inductance has been considered to be 0.2 pu for the purpose of considering a weak grid. The P-I compensators of the Real Power Control structures of all the DG units (will no longer be saturated) will now control the frequency of the DG units, so that the Real Power delivered (to the MG) by the DG units will now follow the reference command of 1.15 MW (the real power supplied by DG unit-2 can be observed from Fig. 8e). Under steady state condition, the frequencies of the DG units and that of the main grid will be equal. This is a clear indication that perfect synchronization has been achieved (The frequency of DG unit-2 is displayed in Fig. 8i). Under steady state condition, the MG is delivering around 0.55 MW and absorbing around 0.1 MVAR (displayed in Fig. 8d) to the main grid (because the real power delivered by the DG units to the MG is more when compared to the real power drawn by the loads of the MG). The Phase voltages at the PCC and the Phase currents of DG unit-2 are displayed in Fig. 8g and Fig. 8h respectively. From Fig. 8f, it can be clearly observed that the THD of the voltages at the various nodes of the MG have reduced to some extent after the MG is synchronized with the main grid, because of the fact that the main grid has added some stiffness to the MG.

V. Conclusions

In this manuscript a unified control structure for DG units based on VSCs has been presented and studied on two DG units delivering power to a local distribution system (working as a MG). The PCC voltage control and the VSC current control loops in cascade have been able to maintain balanced and sinusoidal voltages at the PCC despite the line currents of the DG unit being unbalanced and distorted. Multiple adaptive P-R controllers are reported for the VSC current control loop. The PCC voltage control consists of two parts — the dq-frame control and the zero sequence control. The Real Power control, the frequency control and the Reactive Power–Voltage droop control structures play a role in deciding the reference commands of the PCC voltage control structure in dq-frame. The DG unit is capable of dealing with the unbalanced as well as non-linear operating conditions (considering unbalance even at harmonic frequencies). Also, an improved control structure employing feed-forward compensation for controlling the bi-directional dc-dc converter has been presented. Extensive simulations in PSCAD/EMTDC have confirmed the usefulness of the proposed controllers.

REFERENCES

[1] Nikos Hatziargyriou, "Microgrids Architectures and Control," *IEEE press*, John Wiley and Sons, 2014.

[2] H. Karimi, H. Nikkhajoei, R. Iravani, "Control of an Electronically-Coupled Distributed Resource Unit Subsequent to an Islanding Event," *IEEE Transactions on Power Delivery*, vol. 23, no. 1, pp. 493–501, Jan 2008.

[3] H. Karimi, A. Yazdani, R. Iravani, "Robust Control of an Autonomous Four Wire Electronically-Coupled Distributed Generation Unit," *IEEE Transactions on Power Delivery*, vol. 26, no. 1, pp. 455–466, Jan 2011.

[4] M. Kumar, S. C. Srivastava,, S. N. Singh, "Control Strategies of a DC Microgrid for Grid Connected and Islanded Operations," *IEEE Transactions on Smart Grid*, vol. 6, no. 4, pp. 1588–1601, July 2015.

[5] M. B. Delghavi, A. Yazdani, "A Unified Control Strategy for Electronically Interfaced Distributed Energy Resources," *IEEE Transactions on Power Delivery*, vol. 27, no. 2, pp. 803–812, Apr 2012.

[6] N. R. Merritt, C. Chakraborty, P. Bajpai, "New Voltage Control Strategies for VSC based DG Units in an Unbalanced Microgrid," *IEEE Transactions on Sustainable Energy*, vol. 8, no. 3, pp.1127–1139, July 2017.

[7] M. B. Delghavi, A. Yazdani, "Islanded-Mode Control of Electronically Coupled Distributed-Resource Units Under Unbalanced and Nonlinear Load Conditions," *IEEE Transactions on Power Delivery*, vol. 26, no. 2, pp. 661–673, Apr 2011.

[8] M. Cucuzzella, G. P. Incremona, A. Ferrara, "Design of Robust Higher Order Sliding Mode Control for Microgrids," *IEEE Journal on emerging and selected topics in circuits and systems*, vol. 5, no. 3, pp. 393–401, Sept 2015.

[9] M. B. Delghavi, S. Shoja-Majidabad, A. Yazdani, "Fractional-Order Sliding-Mode Control of Islanded Distributed Energy Resource Systems," *IEEE Transactions on Sustainable Energy*, vol. 7, no. 4, pp. 1482–1491, Oct 2016.

[10] M. Tabari, A. Yazdani, "Stability of a dc Distribution System for Power System Integration of Plug-In Hybrid Electric Vehicles," *IEEE Transactions on Smart Grid*, vol. 5, no. 5, pp. 2564–2573, Sept 2014.

[11] M. Tabari, A. Yazdani, "A Mathematical Model for Stability Analysis of a DC Distribution System for Power System Integration of Plug-In Electric Vehicles," *IEEE Transactions on Vehicular Technology*, vol. 64, no. 5, pp. 1729–1738, May 2015.

[12] S. Lu, L. Wang, T. Lo, A. V. Prokhorov, "Integration of Wind Power and Wave Power Generation Systems Using a DC Microgrid," *IEEE Transactions on Industry Applications*, vol. 51, no. 4, pp. 2753–2761, July/Aug 2015.

[13] S. K. Kollimalla, M. K. Mishra, N. L. Narasamma, "Design and Analysis of Novel Control Strategy for Battery and Supercapacitor Storage System," *IEEE Transactions on Sustainable Energy*, vol. 5, no. 4, pp. 1137–1144, Oct 2014.

[14] T. Ma, M. H. Cintuglu, O. A. Mohammed, "Control of a Hybrid AC/DC Microgrid Involving Energy Storage and Pulsed Loads," *IEEE Transactions on Industry Applications*, vol. 53, no. 1, pp. 567–575, Jan/Feb 2017.

[15] S. K. Kollimalla, M. K. Mishra, A. Ukil, H. B. Gooi, "DC Grid Voltage Regulation Using New HESS Control Strategy," *IEEE Transactions on Sustainable Energy*, vol. 8, no. 2, pp. 772–781, Apr 2017.

[16] Y. Xia, W. Wei, M. Yu, X. Wang, Y. Peng, "Power Management for a Hybrid AC/DC Microgrid With Multiple Subgrids," *IEEE Transactions on Power Electronics*, vol. 33, no. 4, pp. 3520–3533, Apr 2018.

[17] IEEE PES Distribution System Analysis Subcommittee Radial Test Feeders. [Online]. Available: http://ewh.ieee.org/soc/pes/dsacom/testfeeders/index.html.

[18] M. Chen, G. A. Rincon-Mora, "Accurate Electrical Battery Model Capable of Predicting Runtime and IV Performance," *IEEE Transactions on Energy Conversion*, vol. 21, no. 2, pp. 504–511, June 2006.

[19] Y. A Mahmoud, W. Xiao, H. H. Zeineldin, "A Parameterization Approach for Enhancing PV Model Accuracy," *IEEE Transactions on Industrial Electronics*, vol. 60, no. 12, pp. 5708–5716, Dec 2013.

[20] A. Yazdani, R. Iravani, "Voltage Sourced Converters in Power Systems –Modeling, Control and Applications," *IEEE press*, John Wiley and Sons, Inc, 2010.

[21] M. Savaghebi, A. Jalilian, J. C. Vasquez, J. M. Guerrero, "Autonomous Voltage Unbalance Compensation in an Islanded Droop-Controlled Microgrid," *IEEE Transactions on Industrial Electronics*, vol. 60, no. 4, pp. 1390–1402, Apr 2013.

[22] A. Kuperman, "Proportional-Resonant Current Controllers Design Based on Desired Transient Performance," *IEEE Transactions on Power Electronics*, vol. 30, no. 10, pp. 5341–5345, Oct 2015.

[23] X. Yuan, W. Merk, H. Stemmler, J. Allmeling, "Stationary-Frame Generalized Integrators for Current Control of Active Power Filters With Zero Steady-State Error for Current Harmonics of Concern Under Unbalanced and Distorted Operating Conditions," *IEEE Transactions on Industry Applications*, vol. 38, no. 2, pp. 523–532, Mar/Apr 2002.

[24] R. Teodorescu, M. Liserre, P. Rodriguez, "Grid Converters for Photovoltaic and Wind Power Systems," *IEEE press*, John Wiley and Sons, 2011.

[25] S. B. Kjaer, "Evaluation of the 'Hill Climbing' and the 'Incremental Conductance' Maximum Power Point Trackers for Photovoltaic Power Systems," *IEEE Transactions on Energy Conversion*, vol. 27, no. 4, pp. 922–929, Dec 2012.

[26] D. Sera, L. Mathe, T. Kerekes, S.V. Spataru, R. Teodorescu, "On the Perturb-and-Observe and Incremental Conductance MPPT Methods for PV Systems," *IEEE Journal of Photovoltaics*, vol. 3, no. 3, pp. 1070–1078, Jul 2013.

APPENDIX

TABLE A1: Non-linear load at node-844

Transformer	Voltage Ratio	24900/ 480 V
	kVA Rating	500 kVA
	Base Frequency	60 Hz
	Winding Type	Δ/ Y–Gr
	Copper losses	0.019 pu
	Leakage Reactance	0.0408 pu
Diode Rectifier	Type	Single Phase
	Device ON Resistance $R_{ON_{diode}}$	1 mΩ
	Filter Inductances $L_{fDRa}, L_{fDRb}, L_{fDRc}$	15 mH, 15 mH, 15 mH
	Filter Capacitances $C_{DRa}, C_{DRb}, C_{DRc}$	10 mF, 10 mF, 10 mF
	Load Resistances $R_{loada}, R_{loadb}, R_{loadc}$	0.3527 Ω, 0.5290 Ω, 1.058 Ω

TABLE A2: Compensator Parameters

VSC Current Controller	Fundamental Component	$\tau_{c,1} = 0.0004s$
	Harmonic Components (h^{th} harmonic; h=5,7,.....,37)	$K_{RAc,3} = 210$ (3^{rd} harmonic) $K_{RAc,h} = 471.25$
PCC Voltage Controller	dq-frame controller $(K_{vd}(s), K_{vq}(s))$	1.0
	Zero Sequence controller $(K_{vo}(s))$	1.0
Loop filter of the PLL $(K_{PLL}(s))$		$\left(\frac{15}{1+0.002s}\right)$
Notch Filter of the PLL $\left(F_n(s) = \frac{s^2+\omega_c^2}{s^2+2\delta_d\omega_c s+\omega_c^2}\right)$		$\omega_c = 753.9822$ rad/s; $\delta_d = 0.8$
Frequency Controller $(K_f(s))$		$\left(\frac{1}{0.75s}\right)$
Real Power Controller $(K_{P_L}(s))$		$\left(\frac{2}{3}\right) * \left(\frac{s+1}{s}\right)$
Real Power–Frequency Droop Coefficient $\left(K_{P_{droop}}\right)$		0.083333 Hz/MW
Reactive Power–Voltage Droop Coefficient $\left(K_{Q_{droop}}\right)$		13.6 V/MVAR
Buck-Boost Converter Controller $(K_{MPPT,1}(s), K_{MPPT,2}(s))$		$\left(\frac{0.04}{s}\right)$
Noise filter in the current control loops $(G_{ff}(s))$		$\left(\frac{1}{0.001s+1}\right)$
Bi-directional dc-dc converter controller	Inner Loop Current Controller $(K_{cbt1}(s), K_{cbt2}(s))$	$0.8 * \left(\frac{s+1.25}{s}\right)$
	Outer Loop Voltage Controller $(K_{vbt1}(s), K_{vbt2}(s))$	$10 * \left(\frac{s+0.5}{s}\right)$

This article has been accepted for publication in a future issue of this journal, but has not been fully edited. Content may change prior to final publication. Citation information: DOI 10.1109/TPWRD.2019.2952692, IEEE Transactions on Power Delivery

$$Num_c(s) = s^{14}K_{Pc} + \left[\sum_{i=1}^{7} K_{RAc,(2i-1)}\right] s^{13} + \left[K_{RBc,1} + 455K_{Pc}\omega_{PLL}^2\right] s^{12} + \left[454K_{RBc,1}\omega_{PLL}^2 + 77077K_{Pc}\omega_{PLL}^4\right] s^{10}$$
$$+ \left[454K_{RAc,1} + 446K_{RAc,3} + 430K_{RAc,5} + 406K_{RAc,7} + 374K_{RAc,9} + 334K_{RAc,11} + 286K_{RAc,13}\right]\omega_{PLL}^2 s^{11}$$
$$+ \left[76623K_{RAc,1} + 73063K_{RAc,3} + 66327K_{RAc,5} + 57183K_{RAc,7} + 46783K_{RAc,9} + 36663K_{RAc,11}\right]\omega_{PLL}^4 s^9$$
$$+ \left[28743K_{RAc,13}\right]\omega_{PLL}^4 s^9 + \left[76623K_{RBc,1}\omega_{PLL}^4 + 6092515K_{Pc}\omega_{PLL}^6\right] s^8$$
$$+ \left[6015892K_{RAc,1} + 5434948K_{RAc,3} + 4434340K_{RAc,5} + 3290548K_{RAc,7} + 2302372K_{RAc,9}\right]\omega_{PLL}^6 s^7$$
$$+ \left[1656292K_{RAc,11} + 1234948K_{RAc,13}\right]\omega_{PLL}^6 s^7 + \left[6015892K_{RBc,1}\omega_{PLL}^6 + 230673443K_{Pc}\omega_{PLL}^8\right] s^6$$
$$+ \left[224657551K_{RAc,1} + 181758911K_{RAc,3} + 119814943K_{RAc,5} + 69436591K_{RAc,7} + 43914191K_{RAc,9}\right]\omega_{PLL}^8 s^5$$
$$+ \left[30262111K_{RAc,11} + 21967231K_{RAc,13}\right]\omega_{PLL}^8 s^5$$
$$+ \left[224657551K_{RBc,1}\omega_{PLL}^8 + 3841278805K_{Pc}\omega_{PLL}^{10}\right] s^4 + \left[3616621254K_{RBc,1}\omega_{PLL}^{10} + 21878089479K_{Pc}\omega_{PLL}^{12}\right] s^2$$
$$+ \left[3616621254K_{RAc,1} + 2205448606K_{RAc,3} + 845905230K_{RAc,5} + 438885846K_{RAc,7}\right]\omega_{PLL}^{10} s^3$$
$$+ \left[252593254K_{RAc,9} + 179563374K_{RAc,11} + 128816766K_{RAc,13}\right]\omega_{PLL}^{10} s^3$$
$$+ \left[18261468225K_{RAc,1} + 2029052025K_{RAc,3} + 730458729K_{RAc,5} + 372683025K_{RAc,7} + 225450225K_{RAc,9}\right]\omega_{PLL}^{12} s$$
$$+ \left[150921225K_{RAc,11} + 108056025K_{RAc,13}\right]\omega_{PLL}^{12} s + 18261468225\omega_{PLL}^{12}\left[K_{RBc,1} + K_{Pc}\omega_{PLL}^2\right] \quad \text{(A1)}$$

$$Den_c(s) = \left[L_f s + (R_f + 2R_{ON})\right]\left[s^{14} + 455\omega_{PLL}^2 s^{12} + 77077\omega_{PLL}^4 s^{10} + 6092515\omega_{PLL}^6 s^8 + 230673443\omega_{PLL}^8 s^6\right]$$
$$+ \left[L_f s + (R_f + 2R_{ON})\right]\left[3841278805\omega_{PLL}^{10} s^4 + 21878089479\omega_{PLL}^{12} s^2 + 18261468225\omega_{PLL}^{14}\right] + Num_c(s) \quad \text{(A2)}$$

TABLE A3: DG unit Parameters

PV Arrays	Total Capacity (PV Array-1 & 2 combined)		2.3 MW (n_p=240; n_s=48)
	Open Circuit Voltage per module ($V_{oc_{PV}}$)		36 V
	Short Circuit Current per module ($I_{sc_{PV}}$)		8.44 A
	Maximum Power Point (for each module)	Current (I_{MPP})	7.65 A
		Voltage (V_{MPP})	26.74 V
Buck-Boost Converters	R_{fpv1}, R_{fpv2}		0.25 mΩ, 0.25 mΩ
	L_{fpv1}, L_{fpv2}		0.003 H, 0.003 H
	C_{DC1}, C_{DC2}		20000 μF, 20000 μF
	IGBT ON Resistance ($R_{ON_{DC}}$)		0.25 mΩ
Bi-directional dc-dc Converters	R_{fbt1}, R_{fbt2}		0.25 mΩ, 0.25 mΩ
	L_{fbt1}, L_{fbt2}		0.4 mH, 0.4 mH
	IGBT ON Resistance ($R_{ON_{DC}}$)		0.25 mΩ
Battery Energy Storage Systems (BESS-1 and BESS-2)	Rated Voltage ($V_{OC1_{rated}}$, $V_{OC2_{rated}}$)		440 V, 440 V
	R_{SD1}, R_{SD2}		∞, ∞
	C_{C1}, C_{C2}		112910400 F, 112910400 F
	R_{Se1}, R_{Se2}		0.2613 mΩ, 0.2613 mΩ
	R_{TS1}, R_{TS2}		0.0586 mΩ, 0.0586 mΩ
	C_{TS1}, C_{TS2}		200615.55 F, 200615.55 F
	R_{TL1}, R_{TL2}		0.175 mΩ, 0.175 mΩ
	C_{TL1}, C_{TL2}		1275944.55 F, 1275944.55 F
Coupling Transformer	Winding Type		Y–Gr/ Y–Gr
	MVA Rating		1.65 MVA
	Voltage Ratio		0.48/ 24.9 kV
	Base Frequency		60 Hz
	Leakage Reactance		0.1 pu
Voltage Source Converter (VSC)	DC link Capacitances (C_1, C_2)		0.2 F, 0.2 F
	Rated Current (I_{rated})		2 kA (rms)
	IGBT ON Resistance (R_{ON})		0.25 mΩ
	R_{ls1}, R_{ls2}		∞, ∞
	Filter Capacitance (C_f)		0.4 mF
	Filter Inductance		R_f = 0.5 mΩ, L_f = 0.3 mH

Noel Richard Merritt was born on November 22, 1987 in Vijayawada, India. He received the B.Tech degree in Electrical and Electronics engineering from Koneru Lakshmaiah College of Engineering (now Koneru Lakshmaiah University), Guntur, India in 2009 and the M.Tech degree in Power System Engineering from the Indian Institute of Technology Kharagpur, Kharagpur, India, in 2011. He is currently working toward the Ph.D. degree in the Department of Electrical Engineering, Indian Institute of Technology Kharagpur. His research interests include integration of power electronic converters in power systems, Microgrids, HVDC transmission & FACTS controllers.

Chandan Chakraborty (S'92–M'97–SM'01–F'15) received B.E and M.E degrees in Electrical Engineering from Jadavpur University in 1987 and 1989 respectively and Ph.D degrees from Indian Institute of Technology Kharagpur and Mie University, Japan in 1997 and 2000 respectively. Presently, he is a professor in the Department of Electrical Engineering, Indian Institute of Technology Kharagpur. His research interest includes power converters, motor drives, electric vehicles and renewable energy. Dr. Chakraborty was awarded the JSPS Fellowship to work at the University of Tokyo during 2000-2002. He has received the IEEE Bimal Bose Energy Systems Award in 2019. He has regularly contributed to IES conferences such as IECON, ISIE and ICIT as technical program chair/track chair. He is the Founding Editor-in-Chief of IE Technology News (ITeN), a web-only publication for IEEE Industrial Electronics Society. He has served as a Co-EIC of IEEE Transactions on Industrial Electronics during 2018-19. He is appointed as the Founding Editor-in-Chief of IEEE Journal of Emerging and Selected Topics in Industrial Electronics (JESTIE). He is a Fellow of Indian National Academy of Engineering (INAE).

Prabodh Bajpai (M'07–SM'16) received B.E degree from University of Roorkee (now IIT Roorkee) in Electrical Engineering and M.Tech. degree from IIT Delhi in Energy studies in 1997 and 2001 respectively. He has received Ph.D. degree in Electrical Engineering in 2008 from IIT Kanpur, India. He is currently working as Associate Professor in the Department of Electrical Engineering at IIT Kharagpur, India. He was awarded BASE Fellowship from DST, MHRD India to work at University of Washington, USA during 2015. His research interest includes power system restructuring, renewable energy systems, and power system optimization.

Bikash C. Pal (M'00–SM'02–F'13) received B.E.E (with honors) degree from Jadavpur University, Calcutta, India, M.E. degree from the Indian Institute of Science, Bangalore, India, and Ph.D. degree from Imperial College London, London, U.K, in 1990, 1992, and 1999 respectively all in electrical engineering. Currently, he is a Professor in the Department of Electrical and Electronic Engineering, Imperial College London. His current research interests include renewable energy modelling and control, state estimation and power system dynamics. He is Vice President Publications, IEEE Power & Energy Society. He was Editor-in-Chief of IEEE Transactions on Sustainable Energy (2012-2017) and Editor-in-Chief of IET Generation, Transmission and Distribution (2005-2012) and is a Fellow of IEEE for his contribution to power system stability and control.